JACS
JOURNAL OF THE AMERICAN CHEMICAL SOCIETY
Communication
pubs.acs.org/JACS

Elusive β-Zn_8Sb_7: A New Zinc Antimonide Thermoelectric

Jian Wang and Kirill Kovnir*

Department of Chemistry, University of California, Davis, One Shields Avenue, Davis, California 95616, United States

Supporting Information

ABSTRACT: Zn_8Sb_7 was theoretically predicted to exhibit superior thermoelectric properties; however a crystalline phase with a similar composition was only stabilized in the form of nanoparticles. We report a new metastable compound, β-Zn_8Sb_7, which was synthesized in the form of bulk polycrystalline powder via high-temperature solid-state annealing followed by quenching. Single crystal X-ray diffraction indicates that β-Zn_8Sb_7 crystallizes in a new structure type (noncentrosymmetric orthorhombic space group $Pmn2_1$ (no. 31) with unit cell parameters of a = 15.029(1) Å, b = 7.7310(5) Å, c = 12.7431(9) Å, which is different from the nanoparticulate phase. According to differential scanning calorimetry, the β-Zn_8Sb_7 phase melts incongruently at 825(5) K. β-Zn_8Sb_7 is a p-type semiconductor with high Seebeck thermopower and low thermal conductivity stemming from the complex crystal structure. β-Zn_8Sb_7 exhibits a promising thermoelectric figure-of-merit, zT, of 0.33 at 400 K, which is comparable to the state-of-the-art thermoelectric materials based on binary zinc antimonides.

Thermoelectric materials play an important role in renewal energy applications, since they can convert heat into electrical power and *vice versa*.[1,2] The performance of a thermoelectric material is evaluated through the dimensionless figure-of-merit $zT = S^2T/\rho\kappa$, where S is the Seebeck thermopower, T is the absolute temperature, ρ is the electrical resistivity, and κ is the thermal conductivity. Certain drawbacks of current materials prompted extensive search of new materials with high efficiency, low toxicity, low cost, and high stability. Among many potential systems, including clathrates,[3] skutterudites,[4] Heusler and half-Heusler alloys,[5] $A_{14}MSb_{11}$-type antimonides,[6] and chalcogenides,[7] the Zn−Sb system was intensively investigated due to the abundance, low cost and low toxicity of raw materials and promising thermoelectric characteristics. Three compounds in the narrow range of 50−60 atomic % of Zn were reported in the binary Zn−Sb phase diagram: ZnSb,[8] Zn_4Sb_3 (which is actually $Zn_{13}Sb_{10}$),[9] and Zn_3Sb_2.[10] Zn_3Sb_2 is metastable phase at room temperature. In turn, both Zn_4Sb_3 and ZnSb are stable phases with superior thermoelectric characteristics. Recently a new phase, $Zn_{8-\delta}Sb_7$ ($\delta \approx 0.5$), was first discovered in the form of solution-produced nanoparticles[11] and then computationally predicted to be a promising thermoelectric material.[12] We will refer to the previously reported $Zn_{8-\delta}Sb_7$ as the α-Zn_8Sb_7 phase. The challenging task of crystal structure determination of nanoparticles was elegantly solved for α-Zn_8Sb_7 through the combination of automated electron diffraction tomography with precession electron diffraction on individual nanoparticle grains.[11] To the best of our knowledge, neither the crystal structure determined from single crystal diffraction experiments nor experimental data regarding the thermoelectric performance of Zn_8Sb_7 were reported. In this work we present the synthesis of bulk samples of β-Zn_8Sb_7, its crystal structure, which is different than that reported for nanoparticulate α-Zn_8Sb_7, the thermal stability, and thermoelectric properties.

β-Zn_8Sb_7 was first obtained from a reaction of La, Sb, and $ZnCl_2$ (see Supporting Information (SI) for details). Single crystal X-ray diffraction (XRD) experiment revealed the La- and Cl-free composition of Zn_8Sb_7, which was confirmed by energy dispersive X-ray analysis, EDX (Figure 1 and Table S4). The quantitative microprobe analysis confirmed the composition of the new phase to be $Zn_{8.02(6)}Sb_{6.98(6)}$ (Table S5 and Figure S1). Samples containing β-Zn_8Sb_7 as the main phase were also synthesized by high-temperature annealing of the stoichiometric mixture of elements followed by rapid quenching as described in the SI. Our experiments indicate that the β-Zn_8Sb_7 phase has a narrow stability range. Quenching the reaction mixture from 923(5) K resulted in the formation of mainly β-Zn_8Sb_7, while quenching from either 898(5) or 948(5) K did not result in the formation of any considerable amounts of the β-Zn_8Sb_7 phase (Figure 1 and Table S1). In contrast to quenching experiments, differential scanning calorimetry (DSC) performed in evacuated and sealed silica tubes shows that β-Zn_8Sb_7 melts incongruently, decomposing into a mixture of ZnSb and $Zn_{13}Sb_{10}$ already at 825(5) K (Figure 1). The *in situ* XRD experiments to clarify the temperature stability range for β-Zn_8Sb_7 are currently underway. Since the synthesis using the direct reaction of elements was only possible upon quenching from a narrow range of reaction temperatures (Table S1), β-Zn_8Sb_7 is believed to be a metastable phase at room temperature. For the α-Zn_8Sb_7 phase, a metastability at room temperature was computationally predicted.[12]

β-Zn_8Sb_7 crystallizes in a noncentrosymmetric orthorhombic space group $Pmn2_1$ (no. 31, Z = 4) (Table 1). All tested crystals exhibited a tendency for twinning. The structure of β-Zn_8Sb_7 (Figure 2) contains an anionic framework composed of 28 Sb atoms, including 10 Sb_2^{4-} dumbbells and 8 isolated Sb^{3-} anions, leading to a total charge of −64. Thirty-two Zn^{2+} cations compensate the anionic charge resulting in an electron balanced composition (Table S2). Twenty-four Zn atoms are distributed over 6 fully occupied Zn crystallographic sites, while the remaining 8 Zn atoms are distributed over 4 sites with partial occupancies (shown in red in Figure 2A). The Zn−Zn distances shown by red dashed lines are in the range of 1.2−1.4 Å. Thus, only one of two possible Zn atoms shown in red is present. In

Received: August 4, 2015
Published: September 15, 2015

DOI: 10.1021/jacs.5b08214
J. Am. Chem. Soc. 2015, 137, 12474−12477

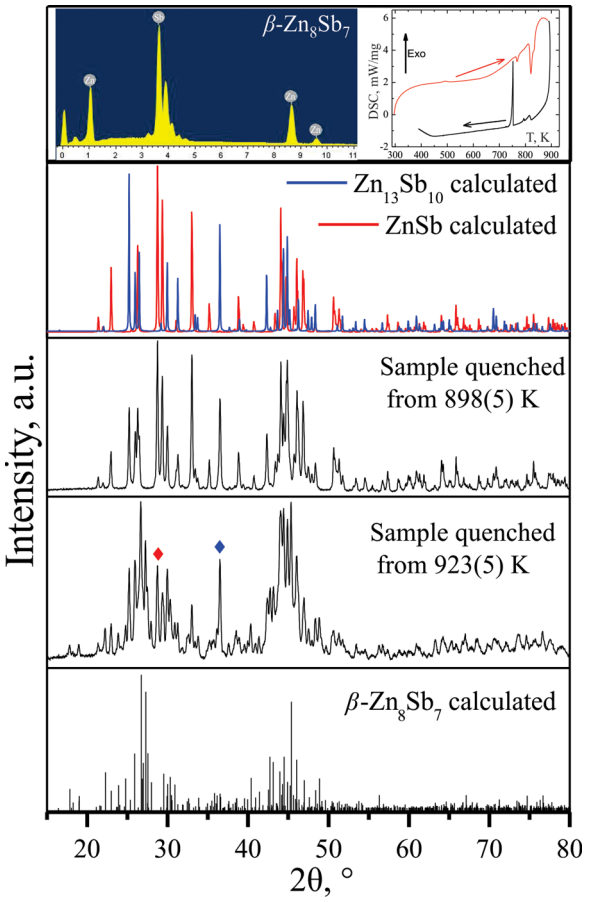

Figure 1. Top: EDX and DSC characterization plots of β-Zn_8Sb_7. Below: experimental powder XRD patterns of samples with the nominal composition Zn_8Sb_7 quenched from 898(5) K and 923(5) K. The calculated patterns for ZnSb (red), $Zn_{13}Sb_{10}$ (blue), and β-Zn_8Sb_7 (black) are also shown. The strongest admixture peaks in sample quenched from 923(5) K are indicated with symbols of corresponding color.

Table 1. Parameters for Data Collection and Refinement for β-Zn_8Sb_7

composition	Zn_8Sb_7	Z	4
space group	$Pmn2_1$ (no. 31)	ρ [g cm^{-3}]	6.17
CSD no.	429936	μ [mm^{-1}]	25.18
temp. [K]	90(2)	data/param.	2710/155
a [Å]	15.029(1)	R_1/wR_2, ($I > 2\sigma(I)$)	0.046/0.117
b [Å]	7.7310(5)		
c [Å]	12.7431(9)	goodness-of-fit	1.34
V [Å^3]	1480.6(2)	diff. peak and hole [e/Å^3]	2.78 and −2.88

each Zn−Zn split pair of atoms, one Zn site has occupancy factor of ~75%, while another Zn atomic position has occupancy factor of ~25% (Table S2). Each Zn atom is surrounded by a distorted tetrahedron of antimony atoms as shown in Figure 2B. Those tetrahedra share common edges and vertices forming a 3D framework. Each partially occupied Zn atomic position shown in red in Figure 2A is situated inside a separate, strongly distorted, Sb_4 tetrahedron (shown in pink in Figure 2B). Two pink tetrahedra around a split pair of Zn atoms share a common face.

β-Zn_8Sb_7 contains both Sb_2^{4-} dumbbells and isolated Sb^{3-} anions, which is similar to $Zn_{13}Sb_{10}$, and different from ZnSb. In the latter compound only Sb_2^{4-} dumbbells are present (Table S6). The Sb−Sb distances within the Sb_2^{4-} dumbbells in β-Zn_8Sb_7 are in the range of 2.80−2.85 Å, which is close to the Sb−Sb distances in ZnSb (2.80 Å),[9a] $Zn_{13}Sb_{10}$ (2.65−3.06 Å),[9h] α-Zn_8Sb_7 (2.72 Å to 2.91 Å)[11] as well as in ternary and quaternary compounds such as $Ca_5Ga_2Sb_6$ (2.84 Å),[13a] $DyCuSb_2$ (2.65 Å),[13b] and $Ca_{10}LaCdSb_9$ (2.84 Å).[13c] In the crystal structure of β-Zn_8Sb_7 the Sb_2^{4-} dumbbells are arranged in noncentrosymmetric way, while Zn sublattice is centrosymmetric and positions of only Zn atoms can be described in the *Pmna* space group, which is a minimal nonisomorphic centrosymmetric supergroup of $Pmn2_1$. The Zn−Sb distances in β-Zn_8Sb_7 are in the range of 2.63−2.85 Å for fully occupied Zn sites. The Zn−Sb distances for the interstitial disordered Zn sites (red atoms and pink polyhedra in Figures 2A,B) span the longer range of 2.58−3.15 Å. This is comparable with the Zn−Sb distances in $Zn_{13}Sb_{10}$ (2.52−3.18 Å),[9h] ZnSb (2.64−2.90 Å),[9a] α-Zn_8Sb_7 (2.66 Å to 3.07 Å)[11] and ternary compounds $Ru_9Zn_7Sb_8$ (2.98−3.26 Å)[14a] and $Fe_{7.77}Zn_{6.73}Sb_9$ (2.92−3.16 Å).[14b] The presence of the disordered interstitial Zn sites was proposed to be the main reason for the low thermal conductivity and, correspondingly, good thermoelectric performance of $Zn_{13}Sb_{10}$. Similar low thermal conductivity was observed for β-Zn_8Sb_7 (*vide infra*).

It is important to compare the structure of β-Zn_8Sb_7 (space group $Pmn2_1$) with the previously reported α-Zn_8Sb_7 phase (space group $P\bar{1}$) that was synthesized via a solution method in the form of nanoparticles as well as with structures of other

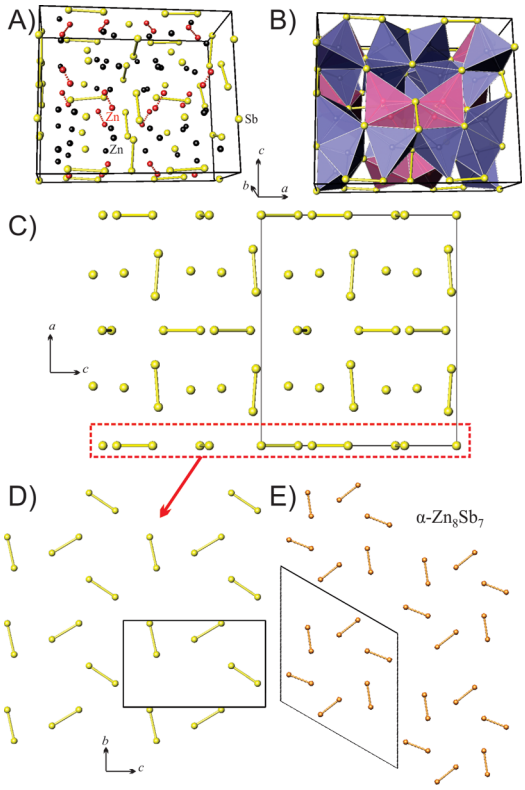

Figure 2. Crystal structure of β-Zn_8Sb_7: (A) a general view with Sb atoms shown in yellow, Zn atoms shown in black, and split Zn positions shown in red with dashed lines indicating short, physically impossible, Zn−Zn distances; (B) polyhedral representation with regular Zn@Sb_4 tetrahedra shown in blue and tetrahedra around the split Zn positions shown in pink; (C) [010] projection of the Sb sublattice; (D) one [100] Sb layer corresponding to the red rectangle highlighted in (C); and (E) an idealized hexagonal packing of Sb_2^{4-} dumbbells in α-Zn_8Sb_7 (orange) for comparison. Unit cells are shown as black lines.

DOI: 10.1021/jacs.5b08214
J. Am. Chem. Soc. 2015, 137, 12474−12477

Table 2. A Comparison of the Transport Properties for Binary Zn−Sb Compounds[a]

comp.	S (μV K^{-1})	ρ (mΩ·cm)	κ (Wm^{-1} K^{-1})	κ_L (Wm^{-1} K^{-1})	zT	N (cm^{-3})	ref
ZnSb	360	62	2.0	1.5	0.04	10^{18}−10^{19}	8c
ZnSb	284	6.6	1.3	0.8	0.37	1.2×10^{18} at 300 K	8d
$Zn_{13}Sb_{10}$	137	2.8	0.75	0.50	0.36	9×10^{19} at 300 K	9f
$Zn_{13}Sb_{10}$	140	2.5	0.75	0.50	0.40	7−9×10^{19} at 300 K	9g
β-Zn_8Sb_7	275	15	0.60	0.55	0.33	5.2×10^{18}	this work
ZnSb + $Zn_{13}Sb_{10}$	150	–	1.0	–	–	–	this work

[a]Unless a different temperature is specified the data are shown for 400 K.

binary zinc antimonides. In the structure of $Zn_{13}Sb_{10}$ all Sb_2^{4-} dumbbells are oriented along one crystallographic direction (Table S6). In turn, in the crystal structure of β-Zn_8Sb_7 the Sb_2^{4-} dumbbells have two orientations, in the [100] plane and almost perpendicular to this plane (Figure 2C). Similar arrangements of Sb_2^{4-} dumbbells were reported for α-Zn_8Sb_7 (Table S6). However, the relative arrangement of those dumbbells in the plane is different in the β-Zn_8Sb_7 and α-Zn_8Sb_7 crystal structures. In the latter structure, the dumbbells are oriented in an almost hexagonal fashion with pseudo six-fold rotational axis running perpendicular to the layer (Figure 2E). The pseudohexagonal symmetry is clearly absent in the structure of β-Zn_8Sb_7 (Figure 2D). The $Zn_{13}Sb_{10}$ phase exhibits polymorphism with the α- and β-phases having different crystal structures and symmetries due to an order−disorder transition in the Zn sublattices. It is possible that the Zn_8Sb_7 phase also has several polymorphic modifications. Moreover, the compositions of β-Zn_8Sb_7 and α-Zn_8Sb_7 are not identical. While β-Zn_8Sb_7 is a stoichiometric compound, a Zn deficiency was proposed for α-Zn_8Sb_7 resulting in a composition of $Zn_{7.5}Sb_7$.[11] Among all binary zinc antimonides, the α-Zn_8Sb_7 phase exhibits anomalously high volume per one atom (Table S6), indicating that the surface energy may play substantial role in the stabilization of the α-form.[12]

The β-Zn_8Sb_7 sample used for properties characterization was contaminated with admixtures of ZnSb and $Zn_{13}Sb_{10}$. This indicates that even upon fast quenching partial decomposition of β-Zn_8Sb_7 occurs. To ensure that the measured properties are due to β-Zn_8Sb_7, a control sample was synthesized by quenching from 898(5) K which appeared to be a mixture of ZnSb and $Zn_{13}Sb_{10}$ in a 11:1 ratio resulting in the nominal composition Zn_8Sb_7 (Tables 2 and S1).

The resistivity of β-Zn_8Sb_7 decreases almost linearly with increasing temperature in the whole temperature range. This behavior is typical for heavily doped semiconductors (Figure 3, top right). The kink in the resistivity dependence of β-Zn_8Sb_7 around 250 K is due to a phase transition of the $Zn_{13}Sb_{10}$ admixture.[9b] The value of resistivity at 400 K of β-Zn_8Sb_7 (15 mΩ·cm) is comparable with the range of resistivity values reported for different ZnSb samples (6.6−62 mΩ·cm) but larger than the resistivity of $Zn_{13}Sb_{10}$ (<3 mΩ·cm) (Table 2). The resistivity of a semiconductor is determined by the following equation: $1/\rho = n \cdot e \cdot \mu$, where n is the carrier concentration; μ is carrier mobility; and e is the charge of an electron. Hall measurements reveal that the carrier concentration of β-Zn_8Sb_7 is 5.2×10^{18} cm^{-3} at 400 K (Figure S3), which is comparable to the carrier concentration in ZnSb (10^{18}−10^{19} cm^{-3})[8c,d] but almost an order of magnitude lower than the carrier concentration in $Zn_{13}Sb_{10}$ (>10^{19} cm^{-3}).[9f,g] A carrier mobility for β-Zn_8Sb_7 (80 cm^2 V^{-1} s^{-1}) is in between the values reported for $Zn_{13}Sb_{10}$ (<30 cm^2 V^{-1} s^{-1}) and ZnSb (>100 cm^2 V^{-1} s^{-1}). As expected from the low carrier concentration, the Seebeck

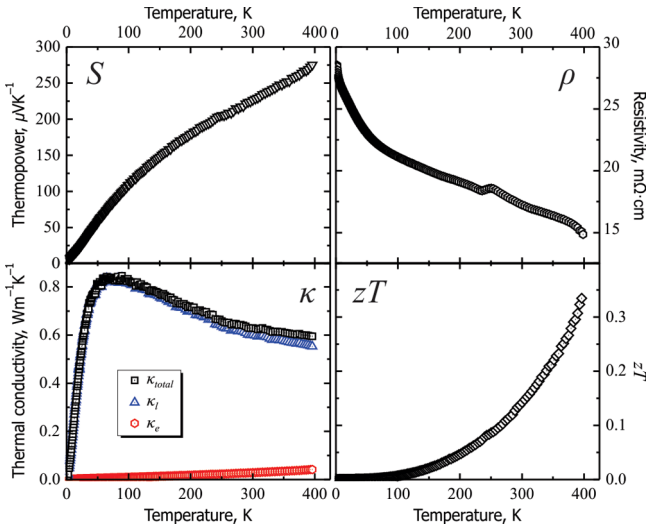

Figure 3. Thermoelectric properties of β-Zn_8Sb_7: (top left) Seebeck thermopower; (top right) electrical resistivity; (bottom left) thermal conductivity with lattice and electronic contributions; (bottom right) thermoelectric figure-of-merit, zT.

thermopower of β-Zn_8Sb_7 (275 μV K^{-1} at 400 K) is significantly higher than the thermopower of $Zn_{13}Sb_{10}$ (140 μV K^{-1}) and comparable to the thermopower of ZnSb (284 μV K^{-1}). The control sample of the $Zn_{13}Sb_{10}$/ZnSb = 1:11 mixture exhibits a much lower thermopower of 150 μV K^{-1}at 400 K (Table 2 and Figure S2), which proves that the high Seebeck thermopower and low thermal conductivity are intrinsic for β-Zn_8Sb_7.

The Seebeck thermopower was approximated by computations for the stoichiometric composition of Zn_8Sb_7 in the idealized stoichiometric hexagonal crystal structure (space group $P6/m$) derived from the structure of α-Zn_8Sb_7.[12] Thermopower values above 250 μV K^{-1} were computed for a charge carrier concentration of 5×10^{19} cm^{-3}. For the β-Zn_8Sb_7 phase we observed similar Seebeck thermopower values at an order of magnitude lower charge carrier concentrations. This demonstrates that tiny differences in the crystal structure may have a high impact on the transport properties.

β-Zn_8Sb_7 inherits the low thermal conductivity of Zn−Sb family due to its intrinsic structural complexity and disorder in the Zn sublattice. β-Zn_8Sb_7 exhibits a total thermal conductivity of 0.60 Wm^{-1} K^{-1} (400 K), which is slightly lower than the thermal conductivity of $Zn_{13}Sb_{10}$ (0.75 Wm^{-1} K^{-1}) and almost three times lower than that of ZnSb (1.3−2.0 Wm^{-1} K^{-1}). The thermal conductivity consists of contributions from charge carriers and phonons, $\kappa_{total} = \kappa_e + \kappa_L = L \cdot T/\rho + \kappa_L$ (κ_e, electronic thermal conductivity; κ_L, lattice thermal conductivity; L, Lorenz number calculated from Seebeck thermopower;[15] ρ, electrical resistivity; T, absolute temperature). The electronic and lattice contributions of the total thermal conductivity of β-Zn_8Sb_7 are

DOI: 10.1021/jacs.5b08214
J. Am. Chem. Soc. 2015, 137, 12474−12477

shown in Figure 3 bottom left. The electronic contribution is relatively small, and the lattice contribution to thermal conductivity dominates. The lattice thermal conductivity of β-Zn_8Sb_7 (0.55 Wm^{-1} K^{-1} at 400 K) is similar to that of $Zn_{13}Sb_{10}$ (0.5 Wm^{-1} K^{-1}) and lower than thermal conductivity for the most of ternary antimonides.[6c] The ultralow lattice thermal conductivity for $Zn_{13}Sb_{10}$ is attributed to the disorder in the Zn sublattice and the presence of the interstitial Zn atoms in the crystal structure.[9d] Disorder in the Zn sublattice is also observed in the crystal structure of β-Zn_8Sb_7, which, in conjunction with the complex crystal structure containing 60 heavy atoms in primitive unit cell, may be responsible for such low lattice thermal conductivity. The combination of high thermopower, ultralow thermal conductivity, and intermediate electrical conductivity of β-Zn_8Sb_7 results in a promising thermoelectric figure-of-merit, zT, of 0.33 at 400 K, which is comparable to ZnSb and $Zn_{13}Sb_{10}$ (Table 2). β-Zn_8Sb_7 has potential for the properties optimization. Studies of the high-temperature properties and charge carrier concentration adjustment via doping are currently underway. The results described here illustrate that the Zn−Sb binary system is surprisingly diverse and far from being fully characterized. New metastable phases with promising thermoelectric properties may arise from Zn−Sb system, as was demonstrated in recent reports of a yet another metastable phase with composition close to Zn_9Sb_7[16a] and the high-temperature stability region for $Zn_{13}Sb_{10}$.[16b]

■ ASSOCIATED CONTENT

Supporting Information

. The Supporting Information is available free of charge on the ACS Publications website at DOI: 10.1021/jacs.5b08214.

Experimental details, EDX and microprobe results, thermoelectric properties of ZnSb+$Zn_{13}Sb_{10}$ sample, Hall effect measurement data (PDF)
Crystallographic data (CIF)

■ AUTHOR INFORMATION

Corresponding Author

*kkovnir@ucdavis.edu

Notes

The authors declare no competing financial interest.

■ ACKNOWLEDGMENTS

The authors would like to thank Kathleen Lee for help with EDX measurements and useful discussion of the manuscript and Prof. Susan Kauzlarich for access to DSC and SPS. This research is supported by the U.S. Department of Energy, Office of Basic Energy Sciences, Division of Materials Sciences and Engineering under award DE-SC0008931.

■ REFERENCES

(1) (a) Snyder, G. J.; Toberer, E. S. *Nat. Mater.* **2008**, *7*, 105. (b) Rowe, D. M. *Thermoelectrics Handbook: Macro to Nano*; CRC/Taylor & Francis: Boca Raton, FL, 2006.

(2) Sootsman, J. R.; Chung, D. Y.; Kanatzidis, M. G. *Angew. Chem., Int. Ed.* **2009**, *48*, 8616.

(3) (a) Christensen, M.; Johnsen, S.; Iversen, B. B. *Dalton Trans.* **2010**, *39*, 978. (b) Fulmer, J.; Lebedev, O. I.; Roddatis, V. V.; Kaseman, D.; Sen, S.; Dolyniuk, J.; Lee, K.; Olenev, A. V.; Kovnir, K. *J. Am. Chem. Soc.* **2013**, *135*, 12313. (c) *The Physics and Chemistry of Inorganic Clathrates*; Nolas, G. S., Ed.; Springer Science: Dordrecht, 2014.

(4) (a) Sales, B. C.; Mandrus, D.; Williams, R. K. *Science* **1996**, *272*, 1325. (b) Nolas, G. S.; Slack, G. A.; Morelli, D. T.; Tritt, T. M.; Ehrlich, A. C. *J. Appl. Phys.* **1996**, *79*, 4002. (c) Nolas, G. S.; Poon, J.; Kanatzidis, M. G. *MRS Bull.* **2006**, *31*, 199.

(5) (a) Uher, C.; Yang, J.; Hu, S.; Morelli, D. T.; Meisner, G. P. *Phys. Rev. B: Condens. Matter Mater. Phys.* **1999**, *59*, 8615. (b) Birkel, C. S.; Zeier, W. G.; Douglas, J. E.; Lettiere, B. R.; Mills, C. E.; Seward, G.; Birkel, A.; Snedaker, M. L.; Zhang, Y.; Snyder, G. J.; Pollock, T. M.; Seshadri, R.; Stucky, G. D. *Chem. Mater.* **2012**, *24*, 2558. (c) Sahoo, P.; Liu, Y.; Poudeu, P. F. P. *J. Mater. Chem. A* **2014**, *2*, 9298.

(6) (a) Brown, S. R.; Kauzlarich, S. M.; Gascoin, F.; Snyder, G. J. *Chem. Mater.* **2006**, *18*, 1873. (b) Kauzlarich, S. M.; Brown, S. R.; Snyder, G. J. *Dalton Trans.* **2007**, 2099. (c) Toberer, E. S.; May, A. F.; Snyder, G. J. *Chem. Mater.* **2010**, *22*, 624.

(7) (a) Plirdpring, T.; Kurosaki, K.; Kosuga, A.; Day, T.; Firdosy, S.; Ravi, V.; Snyder, G. J.; Harnwunggmoung, A.; Sugahara, T.; Ohishi, Y.; Muta, H.; Yamanaka, S. *Adv. Mater.* **2012**, *24*, 3622. (b) Poudel, B.; Hao, Q.; Ma, Y.; Lan, Y.; Minnich, A.; Yu, B.; Yan, X.; Wang, D.; Muto, A.; Vashaee, D.; Chen, X.; Liu, J.; Dresselhaus, M. S.; Chen, G.; Ren, Z. F. *Science* **2008**, *320*, 634. (c) Biswas, K.; He, J. Q.; Blum, I. D.; Wu, C. I.; Hogan, T. P.; Seidman, D. N.; Dravid, V. P.; Kanatzidis, M. G. *Nature* **2012**, *489*, 414. (d) Zhao, L. D.; Lo, S.-H.; Zhang, Y.; Sun, H.; Tan, G.; Uher, C.; Wolverton, C.; Dravid, V. P.; Kanatzidis, M. G. *Nature* **2014**, *508*, 373.

(8) (a) Almin, K. E. *Acta Chem. Scand.* **1948**, *2*, 400. (b) Valset, K.; Böttger, P. H. M.; Taftø, J.; Finstad, T. G. *J. Appl. Phys.* **2012**, *111*, 023703. (c) Eklöf, D.; Fischer, A.; Wu, Y.; Scheidt, E.-W.; Scherer, W.; Häussermann, U. *J. Mater. Chem. A* **2013**, *1*, 1407. (d) Xiong, D. B.; Okamotoa, N. L.; Inui, H. *Scr. Mater.* **2013**, *69*, 397.

(9) (a) Mozharivskyj, Y.; Pecharsky, A. O.; Bud'ko, S.; Miller, G. J. *Chem. Mater.* **2004**, *16*, 1580. (b) Nylén, J.; Andersson, M.; Lidin, S.; Häussermann, U. *J. Am. Chem. Soc.* **2004**, *126*, 16306. (c) Yin, H.; Blichfeld, A. B.; Christensen, M.; Iversen, B. B. *ACS Appl. Mater. Interfaces* **2014**, *6*, 10542. (d) Snyder, G. F.; Christensen, M.; Nishibori, E.; Caillat, T.; Iversen, B. B. *Nat. Mater.* **2004**, *3*, 458. (e) Ugai, Y. A.; Averbakh, E. A.; Lavrov, V. V. *Phys. Solid State* **1963**, *4*, 2393. (f) Caillat, T.; Fleurial, J.-P.; Borshchevski, A. *J. Phys. Chem. Solids* **1997**, *58*, 1119. (g) Toberer, E. S.; Rauwel, P.; Gariel, S.; Taftø, J.; Snyder, G. J. *J. Mater. Chem.* **2010**, *20*, 9877. (h) Pedersen, B. L.; Birkedal, H.; Nishibori, E.; Bentien, A.; Sakata, M.; Nygren, M.; Frederiksen, P. T.; Iversen, B. B. *Chem. Mater.* **2007**, *19*, 6304.

(10) (a) Li, J. B.; Record, M.-C.; Tedenac, J. C. *J. Alloys Compd.* **2007**, *438*, 171. (b) Massalski, T. B.; Okamoto, H. *ASM International Binary Alloy Phase Diagrams*; ASM International: Materials Park, OH, 1990.

(11) Birkel, C. S.; Mugnaioli, E.; Gorelik, T.; Kolb, U.; Panthöfer, M.; Tremel, W. *J. Am. Chem. Soc.* **2010**, *132*, 9881.

(12) Pomrehn, G. S.; Toberer, E. S.; Snyder, G. J.; Walle, A. *J. Am. Chem. Soc.* **2011**, *133*, 11255.

(13) (a) Cordier, G.; Schaefer, H.; Stelter, M. *Z. Naturforsch. B* **1985**, *40*, 5. (b) Szytula, A.; Kolenda, M.; Oles, A. *J. Alloys Compd.* **2004**, *383*, 224. (c) Wang, J.; Xia, S. Q.; Tao, X. T. *Chem. - Asian J.* **2013**, *8*, 251.

(14) (a) Bang, X. D.; Feng, Z. Y.; Okamoto, N. L.; Pietzonka, C.; Waki, T.; Inui, H. *Inorg. Chem.* **2010**, *49*, 10536. (b) Dingbang, X.; Yufeng, Z. *J. Solid State Chem.* **2011**, *184*, 1159.

(15) Kim, H.-S.; Gibbs, Z. M.; Tang, Y.; Wang, H.; Snyder, G. J. *APL Mater.* **2015**, *3*, 041506.

(16) (a) Mozharivskyj, Y. Oral presentation at North American Solid State Chemistry Conference, Tallahassee, FL, May 22−24, 2015. (b) Lin, J.; Li, X.; Qiao, G.; Wang, Z.; Carrete, J.; Ren, Y.; Ma, L.; Fei, Y.; Yang, B.; Lei, L.; Li, J. *J. Am. Chem. Soc.* **2014**, *136*, 1497.

DOI: 10.1021/jacs.5b08214
J. Am. Chem. Soc. 2015, 137, 12474−12477